Fracture Behavior of Sisal Fiber–Reinforced Starch-Based Composites

V. Alvarez, A. Vázquez, C. Bernal
Research Institute of Material Science and Technology (INTEMA), Engineering Faculty, National University of Mar del Plata, Juan B. Justo 4302 (B7608FDQ), Mar del Plata, Argentina

The fracture behavior of biodegradable fiber–reinforced composites as a function of fiber content under different loading conditions was investigated. Composites with different fiber content, ranging from 5 to 20 wt%, were prepared using commercial starch-based polymer and short sisal fibers. Quasistatic fracture studies as well as instrumented falling weight impact tests were performed on the composites and the plain matrix. Results showed a significant increase in the crack initiation resistance under quasistatic loading. This was caused by the incorporation of sisal fibers to the matrix and the development of failure mechanisms induced by the presence of the fibers. On the other hand, a modest increasing trend of the resistance to crack initiation with fiber loading was detected. An improved fracture behavior was also observed when the impact loading was parallel to the thickness direction. Under these experimental conditions, the composites exhibited higher values of ductility index, energy at initiation and total fracture energy than the plain matrix. Furthermore, an increasing trend of these parameters with fiber content was detected in the biocomposites. Overall, the addition of sisal fibers to the biodegradable matrix appears to be an efficient mean of improving fracture behavior under both quasistatic and impact loading conditions. POLYM. COMPOS., 26:316–323, 2005. © 2005 Society of Plastics Engineers

INTRODUCTION

Reinforcing thermoplastic polymers with natural fibers has become very attractive because of the good mechanical properties that can be obtained at relatively low cost [1]. Currently, the use of natural fibers as reinforcements in industrial applications is specially being considered in the automotive and packaging industries. The use of natural fibers as an alternative of the use of glass fibers in biodegradable matrices is mainly driven by ecological reasons. Several works have been done concerning the use of natural fibers with thermoplastic biodegradable polymers [2–10].

Correspondence to: C. Bernal; e-mail: crbernal@fi.mdp.edu.ar
Contract grant sponsor: CONICET-PICT1208011.
DOI 10.1002/pc.20103
Published online in Wiley InterScience (www.interscience.wiley.com).

Natural fibers are commonly used in the form of discontinuous reinforcements, although natural fiber–reinforced polymers do not offer stiffness and strength values as high as continuous-fiber composites. Their low cost and easy processing make them preferred for many applications [11].

On the other hand, short-fiber–reinforced thermoplastics have a complex microstructure. This is a consequence of the fiber length and orientation distribution in the molding and the existence of the interface, which affects the mechanical properties and the stress concentrations at the fiber ends.

In short-fiber–reinforced composites, a large number of inelastic failure mechanisms in the vicinity of an advancing crack become active. These mechanisms contribute to the creation of the fracture process zone with a concomitant substantial slow crack growth preceding unstable fracture [12, 13].

Different energy dissipation mechanisms can be identified depending on the fiber length. In short-fiber–reinforced thermoplastics, the fibers of subcritical length are pulled out rather than broken, as they are too short to reach their strength. In this case, the relevant energy dissipation mechanisms such as debonding, sliding, restricted pull-out, and brittle or ductile matrix fracture are well described elsewhere [11–13]. Other failure mechanisms (i.e., fiber splitting into ultimate cells, stretching and uncoiling of microfibrils in the cells of fibers, transverse microcracking, and multiple ultimate cell fracture) were also described in natural fiber–reinforced polymers [7, 8].

The fracture characterization of short-fiber–reinforced polymers using fracture mechanics has been studied intensively [11, 12, 14–18]. However, there are relatively few reports on the failure behavior of natural fiber–reinforced biodegradable polymers [7–10].

In this study, we evaluated the fracture behavior of a sisal fiber–reinforced starch-based polymer as a function of fiber content under different loading conditions.

METHODOLOGIES FOR FRACTURE CHARACTERIZATION

The critical stress intensity factor K_{IC}, and the critical elastic strain energy release rate G_{IC}, can be determined by

following the ASTM D 5045-93 recommendations [19]. They represent the intensity of the stress field ahead of the crack tip at fracture initiation and the energy required to initiate fracture, respectively.

The dependence of fracture toughness on composition can be analyzed using the following expressions derived by Pukánszky and Maurer [20]. The changes in properties due to the interaction between components have been considered proportional to the actual values of those properties in this analysis [20]:

$$G_{Ic} = G_{Icm}(E_m/E)(1 - v_f)/(1 + 2.5v_f)\exp(B_{Gc}v_f) \quad (1)$$

$$K_{Ic}^2 = K_{Icm}^2(1 - v_f)/(1 + 2.5v_f)\exp(B_{Kc}v_f) \quad (2)$$

where E_m/E accounts for the inverse correlation that exists between fracture resistance and stiffness of the material and the term $(1 - v_f)/(1 + 2.5v_f)$ represents the change in the effective load-bearing cross-section of the matrix due to the presence of the fibers. B is related to fiber-matrix interface properties [21] and is particular to each system.

The effect of the reduced load bearing cross section can be eliminated, if the reduced properties are plotted against fiber content in the linearized form of *Eqs. 1* and *2*:

$$\ln G_{ICred} = \ln G_{ICm} + B_{GC}v_f \quad (3)$$

$$\ln K_{ICred}^2 = \ln K_{ICm}^2 + B_{KC}v_f \quad (4)$$

From the slope of the linear regression of experimental data, B_{Gc} and B_{Kc} parameters can be easily determined. Their values can be used for determining the effect of component interaction on fracture resistance.

Another approach to characterize crack resistance of materials is the work of fracture, which represents the energy absorbed by the creation of fracture surfaces of completely broken samples. Hence, it involves physical information on the critical load as well as on crack growth [12]. It can be expressed as the total energy supplied to the sample (U) divided by twice the remaining ligament area of the test specimen (A) [22]:

$$w_{of} = U/(2A) \quad (5)$$

This test has the advantage that it does not require any information on the stress intensity of the notch, the material elastic properties, or its mechanical linearity [22].

On the other hand, the material response against impact loads parallel to the thickness direction can be evaluated by the instrumented falling weight impact technique. Impact strength and energy at crack initiation as well as total fracture energy and ductility index can be obtained from impact tests [15].

EXPERIMENTAL

MaterBi-Y®, a commercial starch based polymer, was kindly supplied by Novamont, Novara, Italy. Composites with different fiber content, ranging from 5 to 20 wt%, were prepared using MaterBi-Y® as the matrix and short sisal fibers with an average diameter and length of 220 ± 30 μm and 7.2 ± 0.08 mm, respectively (Brascorda, Brazil). The polymer pellets and the sisal fibers were mixed at 180 °C. After mixing for 20 min, the pellets were compression-molded into plaques at 180 °C and 700 MPa and rapidly cooled down with running water. Finally, the plaques were annealed in an oven for 1 h at 60°C in order to release thermal stresses generated during molding.

It is important to note that fiber fragmentation can be induced during the above procedure. Average diameter and length values of sisal fiber after processing have been reported previously [23] (fiber diameter = 130 ± 50 μm and fiber length = 2.42 ± 0.98 mm). They were measured from optical microscopy after extracting the fibers from matrix with acetone.

Quasistatic fracture characterization was performed on three-point bend specimens (SE(B)) cut out from compression-molded thick plaques (thickness, B = 5 mm) which were machined to reach final dimensions and improve edge surface finishing.

Sharp notches were introduced by sliding a fresh razor blade into a machined slot. Crack-to-depth ratio (a/W) was 0.5. Thickness-to-depth ratio (B/W) and span-to-depth ratio (S/W) were always kept equal to 0.5 and 4, respectively.

Fracture tests were performed in an INSTRON dynamometer 4467 with a crosshead speed of 2 mm/min.

Puncture tests were conducted on disk samples of 90-mm diameter cut out from 3-mm thickness compression-molded plates. These tests were performed in a falling weight Fractovis of Ceast at 1 m/s.

All samples were dried in a vacuum oven at 60°C until constant weight was attained before testing. All tests were carried out at room temperature.

Fracture surfaces of SE(B) samples were characterized by scanning electron microscopy (SEM).

RESULTS AND DISCUSSION

Quasistatic In-Plane Fracture Properties

Figure 1 shows load-displacement traces of the MaterBi-Y® matrix and the composite with 15 wt% of fibers tested in three-point bend configuration. The MaterBi-Y® matrix displayed almost linear load-displacement traces with an abrupt drop of load to zero immediately after crack initiation, revealing the brittle-like behavior of this material. Conversely, the sisal reinforced composites showed higher stiffness and a higher degree of nonlinearity before maximum load caused by irreversible events [24]. A gradual fall of load from the maximum point was observed thereafter, and samples exhibited stable crack propagation. Further-

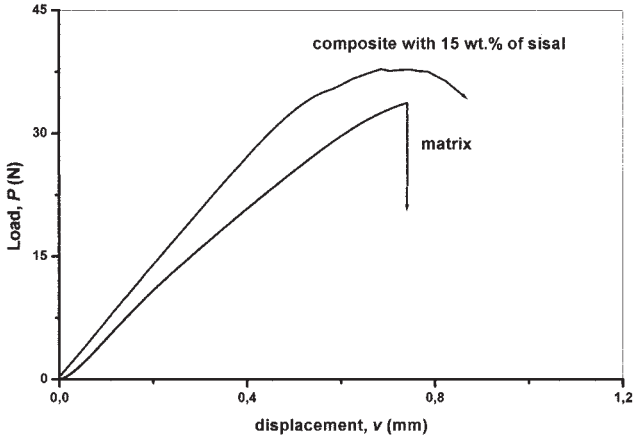

FIG. 1. Load-displacement traces for the MaterBi-Y® matrix and the composite with 10 wt% of sisal fibers.

more, no signs of macroscopic yielding of the matrix were observed on tested samples. Linear elastic fracture mechanics (LEFM) through the stress intensity factor (K_{IQ}) and the strain energy release rate (G_{IQ}) was adopted to characterize the resistance to crack initiation in these materials. These parameters were calculated from the maximum in the load-displacement curves following the procedure described in the ASTM standard [19]. The results are listed in Table 1 along with their deviations. A significant increase in K_{IQ} and G_{IQ} was observed as a result of the addition of sisal fibers to the plain matrix and the development of new failure mechanisms induced by the presence of those fibers. A modest increasing trend of these fracture parameters with fiber loading was also found as a consequence of the increase of these dissipation mechanisms.

The fracture parameter values obtained here did not represent valid plane strain fracture toughness values, since the materials load-displacement behavior was near the limit of validity of LEFM (10% nonlinearity allowance) and the ASTM size requirement for plane strain determinations [19] was not fulfilled (Table 1). However, our fracture parameter values still reflected a critical stress state for crack initiation [25]. (The minimum thickness values B_{min} in Table 1 were calculated using tensile strength values reported in Ref. 26).

The work of fracture approach, which mainly describes the stage of crack propagation [12], was also performed in order to detect any difference in the fracture propagation mode that was not reflected by the fracture initiation parameters [27]. The higher values of the work of fracture exhibited by the composites compared to the unreinforced matrix (Table 1) indicated that the incorporation of sisal fibers to the matrix also improved fracture propagation behavior in our composites. On the other hand, the work of fracture appeared to be independent of sisal fiber content suggesting that no significant differences in the fracture propagation mode existed among these biocomposites.

TABLE 1. In plane fracture properties obtained under quasi-static loading conditions.

Sisal fibers wt%	G_{IQ} (kJ/m^2)	K_{IQ} (MPa · m$^{1/2}$)	B_{min} (mm)	w_{of} (KJ/m^2)
0	0.78 ± 0.12	0.86 ± 0.11	11.6	0.77 ± 0.11
5	1.53 ± 0.09	1.43 ± 0.18	24.6	1.48 ± 0.21
10	1.59 ± 0.11	1.70 ± 0.14	29.3	1.49 ± 0.14
15	1.61 ± 0.12	1.97 ± 0.18	34.4	1.53 ± 0.07
20	1.68 ± 0.16	2.04 ± 0.16	30.7	1.48 ± 0.06

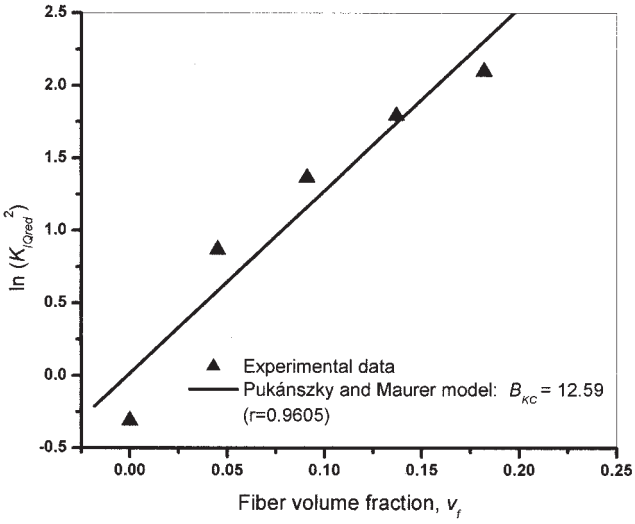

FIG. 2. a: Reduced values of K_{IQ} (MPam$^{1/2}$) plotted in a linearized form according to *Eq. 3*. b: Reduced values of G_{IQ} (KJ/m^2) plotted in a linearized form according to *Eq. 4*.

Figure 2 shows the results obtained from the application of Pukánszky and Maurer model [20] for K_{IQ} and G_{IQ} on our sisal/MaterBi-Y® composites. A substantial linear correlation was obtained for both fracture parameters suggesting that this model successfully fit our experimental data.

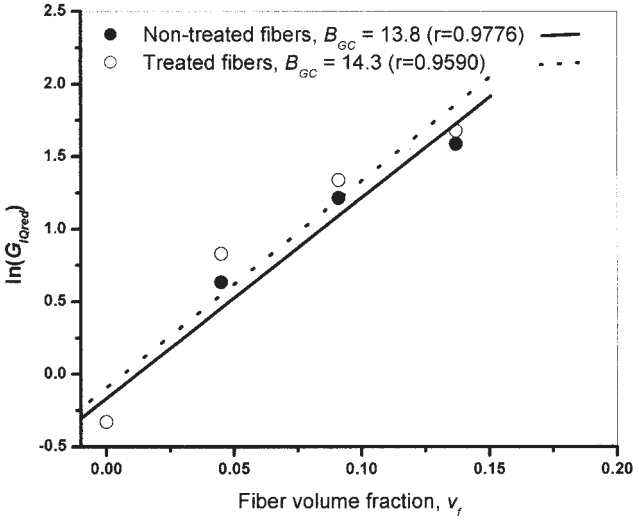

FIG. 3. Reduced values of G_{IQ} (KJ/m^2) plotted in a linearized form according to *Eq. 4* for the impact data reported in literature for the same composites [26].

Therefore, the corresponding parameters B_{Kc} and B_{Gc} could also be used to study the effect of interaction on fracture resistance in these composites. Based on these results, the Pukánszky and Maurer model [20] was also used to fit the impact fracture data previously reported in the literature for the same composites containing treated and nontreated fibers [26]. A substantial linear regression of these data is shown in Fig. 3, (r was 0.9776 and 0.9590 for the composites with nontreated and treated fibers, respectively). Thus, it also confirms the assumption that the Pukánszky and Maurer model [20] can adequately describe the composition dependence of fracture parameters in our composites. However, the difference in the interaction parameter values B_{GC} was within the experimental scatter of impact data, and was unable to quantify the small improvement of fiber-matrix interface properties obtained with alkali treatment of sisal fibers [26].

Impact Out of Plane Fracture Properties

Table 2 shows the values of disk strength, energy at crack initiation, ductility index, and fracture energy of the different composites assayed. A decrease in the disk strength in comparison to the plain matrix was observed for the composite containing up to 15 wt% of sisal fibers. We hypothesize that the fibers spread in the matrix can act as crack initiation points during impact for these compositions [15]. In addition, a regular increasing trend of disk strength with fiber content was observed. Indeed, there were enough fibers at 20 wt% of sisal to enhance load transfer [15]. Conversely, the addition of sisal fibers to the MaterBi-Y® matrix led to a sharp increase in the ductility index (Table 2) as new energy dissipation mechanisms resulting from the presence of the fibers became active. The same effect was observed by Mouzakis et al. [15] with injection molded PP/DLGF composites. For the composites investigated here, the ductility index was found to increase with fiber loading specially for the highest fiber content used (20 wt%).

A similar trend for the energy at initiation and the fracture energy with fiber content was also observed. This result suggests that the incorporation of sisal fibers to the biodegradable matrix is also an efficient way to improve impact fracture properties.

Figure 4 shows the macrophotographs of the opposite side of the impacted areas of the neat polymer and the composites with 10 and 15 wt% of sisal fibers. Many radial cracks were observed around the hole area of the matrix samples (Fig. 4a), whereas in the composites a circumferential cracking became more dominant as fiber content increased (Fig. 4b and c). Mouzakis et al. [15] have pointed out that the circumferential shear-cracking phenomenon is more effective in toughness improvement than radial cracking mechanism. Hence, the increasing trend of fracture energy with fiber content shown in Table 2 could be explained in terms of an increase in the circumferential shear-cracking mechanism as the fiber content increased.

Fracture Surface Analysis

The SEM micrographs of fracture surfaces of SE(B) samples of the composite with 15 wt% of sisal are shown in Fig. 5a–d at different magnifications. In all micrographs, the matrix displayed flat surfaces indicating the absence of any plastic deformation. Furthermore, sisal fibers did not hold the matrix material, suggesting a relatively poor fiber-matrix interface.

The presence of fiber pull-out could be predicted by considering the critical fiber length concept. For short fiber

TABLE 2. Impact out of plane fracture properties.

Sisal fibers wt%	Disk strength, σ (MPa)	Energy at initiation, E_{init} (kJ/m)	Ductility index, $D.I.$	Fracture energy, E_{total} (kJ/m)
0	111.0 ± 5.44	0.17 ± 0.03	0	0.17 ± 0.03
5	80.1 ± 1.43	0.33 ± 0.09	0.14 ± 0.04	0.40 ± 0.13
10	97.1 ± 1.36	0.37 ± 0.03	0.16 ± 0.03	0.43 ± 0.44
15	106.4 ± 1.85	0.37 ± 0.04	0.18 ± 0.05	0.45 ± 0.03
20	129.8 ± 7.59	0.46 ± 0.02	0.24 ± 0.01	0.61 ± 0.03

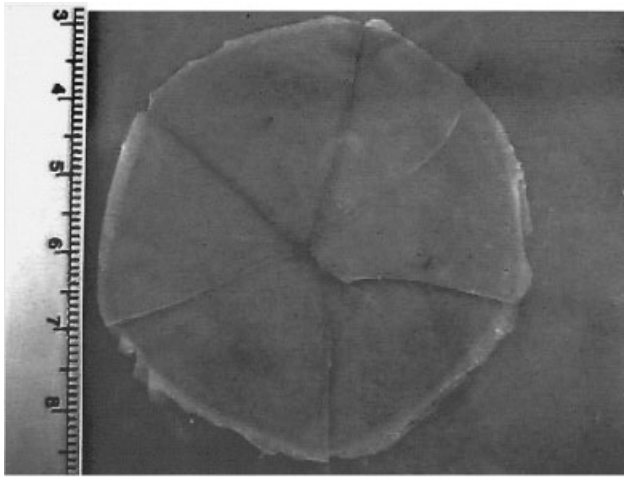

(a)

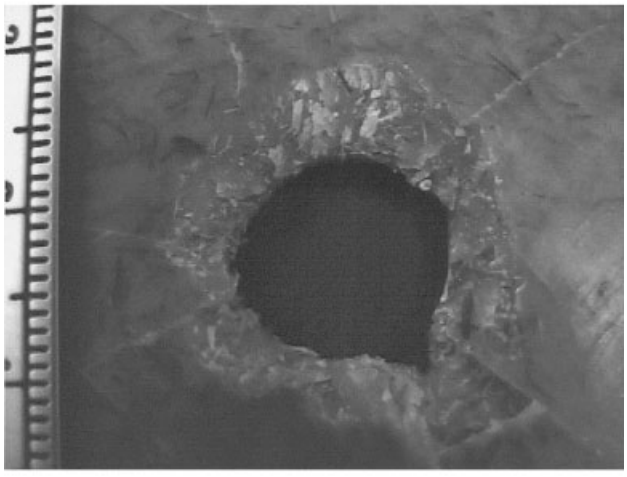

(b)

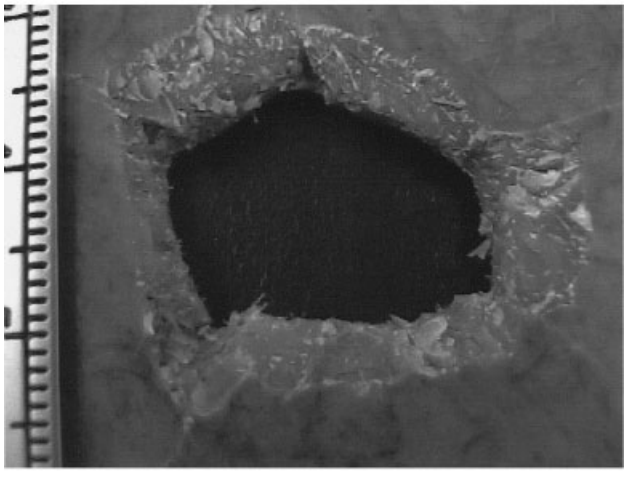

(c)

FIG. 4. Macrophotographs of the opposite of impacted sides. a: MaterBi-Y® matrix. b: Composite with 10 wt% of fibers. c: Composite with 15 wt% of fibers.

reinforced composites, there is effective load transfer from the matrix to the fiber provided a strong fiber-matrix interfacial bond and a fiber length longer than a critical value (L_c) exist [28]. L_c can be estimated by applying the Kelly-Tyson model [29]:

$$L_c = d\sigma_f/2\tau \tag{6}$$

where σ_f is the fiber strength, d is the fiber diameter, and τ is the interfacial shear strength. For the sisal fiber used for preparing our composites, σ_f = 471.6 MPa [26] and for perfectly bonded fibers, τ was assumed to be the shear strength of the matrix, which was 6.3 MPa for MaterBi-Y® [23]. L_c was found to be about 4.9 mm, which was longer than the mean fiber length of the composites after processing ($L \simeq 2.42$ mm). Hence, the fibers were expected to be pulled out rather than broken as they were not able to reach their strength.

Figure 5 shows fiber pull-out (Fig. 5a and b) as well as other energy dissipation mechanisms which are active and produce the increase in toughening. Such mechanisms are: modest fiber-matrix debonding, separation of sisal fibers into ultimate cells by axial splitting of the boundary layer, uncoiling of these spirally arranged microfibrils (Fig. 5c), and microcracking of ultimate cells (Fig. 5d). It has been previously reported by Lu et al. [8] that even uncoiling of microfibrils inside the plant fibers consumes substantial energy and therefore, imparts high mechanical performance to the composite. On the other hand, surface roughness is also clearly observed in Fig. 5. This is due to the organic matrix surrounding the primary cell wall of fibers, which might be responsible of additional energy absorbing mechanisms such us friction and pull-out of ultimate cells [30].

CONCLUSIONS

The fracture behavior of completely biodegradable composites was studied as a function of fiber content under different loading conditions.

Under quasistatic loading, the biocomposites exhibited higher resistance to crack initiation and work of fracture in comparison to the plain matrix. These differences between the composites and the matrix may be due to the development of new energy dissipation mechanisms derived from the presence of the fibers. In addition, the increase of these failure mechanisms may explain the slight increasing trend of the resistance to crack initiation with fiber loading.

The simple model proposed by Pukánszky and Maurer [20] to predict fracture properties in heterogeneous systems was suitable for these sisal/MaterBi-Y® composites.

We have also found that the impact out of plane fracture showed an increasing trend of energy at initiation, ductility index, and total fracture energy proportional to the fiber loading. The total fracture energy response was interpreted

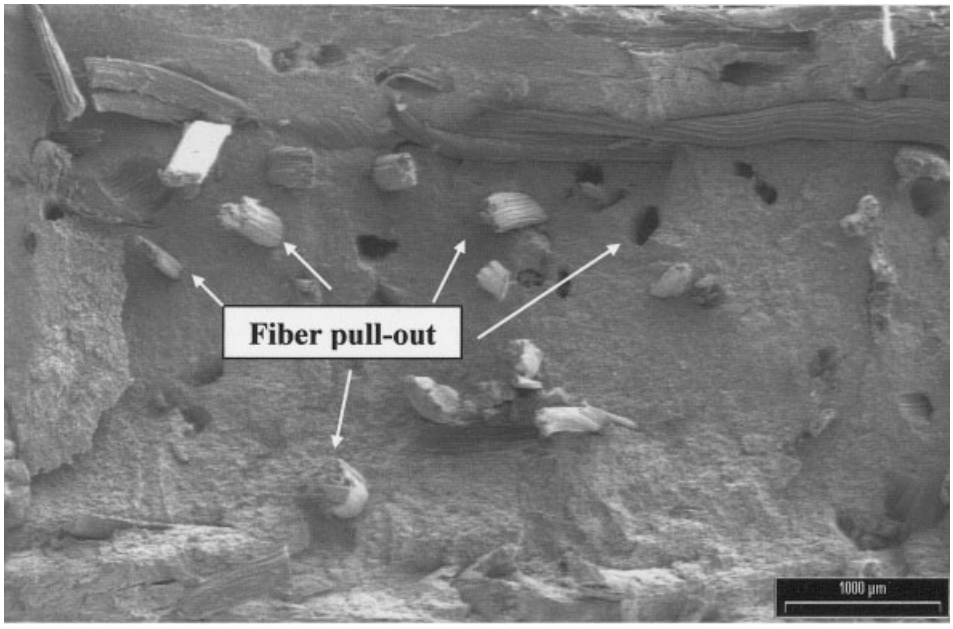

(a)

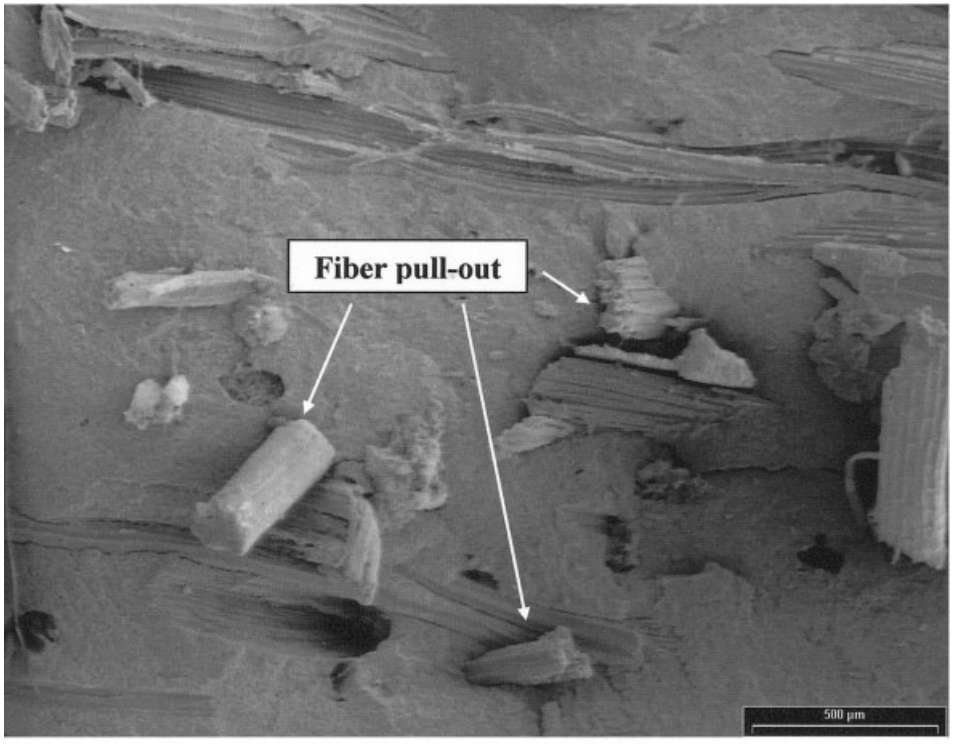

(b)

FIG. 5. SEM micrographs of fracture surfaces of SE(B) samples of the composite with 15 wt% of fibers at different magnifications. a: 20×; b: 48×; c: 100×; d: 500×.

in terms of the increasing circumferential shear-cracking mechanism observed on impacted samples.

The fracture surface analysis suggested that axial splitting of the boundary layer between ultimate cells, uncoiling of microfibrils inside the plant fibers, microcracking, and fiber pull-out were the main failure mechanisms active in these composites.

In conclusion, the results obtained in this study showed that the addition of sisal fibers to the actual biodegradable matrix appears to be an efficient mean of improving fracture

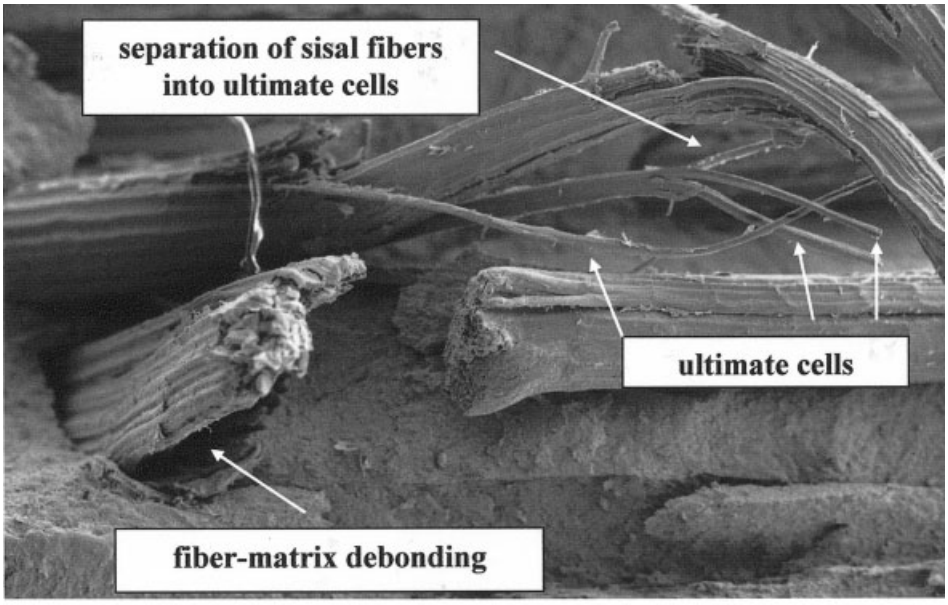

(c)

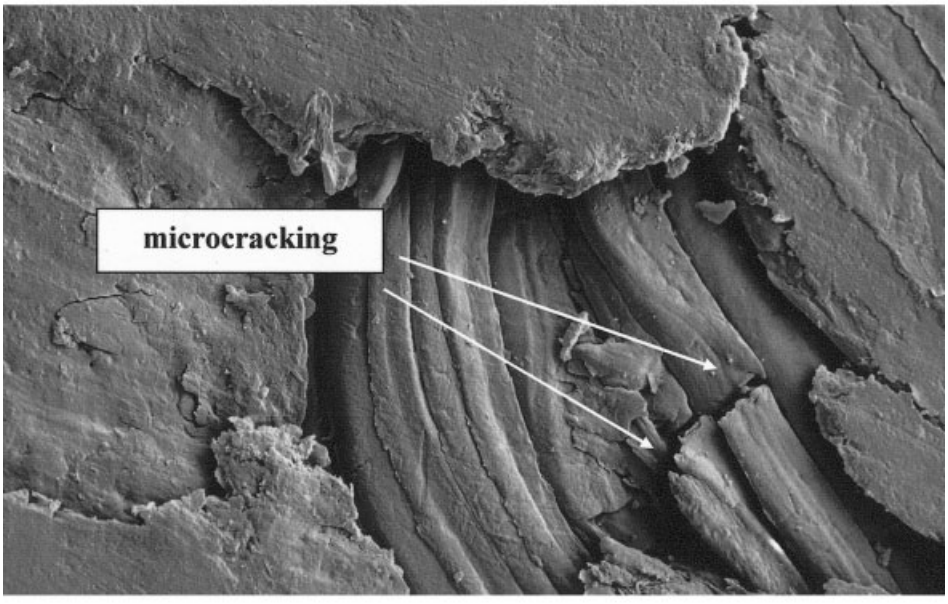

(d)

FIG. 5. (*Continued*)

behavior under both quasistatic and impact loading conditions.

REFERENCES

1. A.K. Bledzki and J. Gassan, *Prog. Polym. Sci.*, **24**, 221 (l999).
2. S. Iannace, L. Nocilla, and L. Nicolais, *J. Appl. Polym. Sci.*, **73**, 585 (1999).
3. H. Hanselka, and A.S. Herrman, "Fiber Properties and Characterization," *7 Internationales Techtexil Symposium*, 20 (1994).
4. A. Dufresne and M.R.Vignon, *Macromolecules*, **31**, 2693 (1998).
5. J. Kuruvilla and L.H.C.Mattoso, "Sisal Fibre Reinforced Polymer Composites: Status and Future," *Third Int. Symposium Natural Polymers and Composites*, 333 (2000).
6. C. Biastioli, *Principles and Applications: Starch-Polymer Composites in Degradable Polymers*, G. Scott and D. Gilead, editors, Chapman & Hall, London (1995).
7. G. Romhány, J. Karger-Kocsis, and T. Czigány, *Macromol. Mater. Eng.*, **288**, 699 (2003).
8. X. Lu, M.Q. Zhang, M.Z. Rong, G. Shi, and G.C. Yang, *Polym. Compos.*, **23**, 624 (2002).

9. X. Lu, M.Q. Zhang, M.Z. Rong, G. Shi, G.C. Yang, and H.M. Zeng, *Adv. Compos. Lett*., **8**, 231 (1999).
10. M. Avella, E. Martuscelli, B. Pascucci, M. Raimo, B. Focher, and A. Marzetti, *J. Appl. Polym. Sci.*, **49**, 2091 (1993).
11. B. Lauke, *J. Polym. Eng*., **11**, 104 (1992).
12. B. Lauke and W. Pompe, *Compos. Sci. Technol*., **26,** 37 (1986).
13. B. Lauke and W. Pompe, *Compos. Sci. Technol*., **31**, 25 (1988).
14. S.-C. Wong and Y.-W. Mai, *Polym. Eng. Sci.*, **39**, 356 (1999).
15. D.E. Mouzakis, T. Harmia, and J. Karger-Kocsis, *Polym. Polym. Comp.*, **8**, 167 (2000).
16. S.-C. Wong, G.-X. Sui, C.-Y. Yue, and Y.-W. Mai, *J. Mat. Sci.*, **37**, 2659 (2002).
17. G.-X. Sui, S.-C. Wong, and C.-Y. Yue, *Compos. Sci. Technol*., **61**, 2481 (2001).
18. S.-C. Tjong, S.-A. Xu, R.K.-Y. Li, and Y.-W. Mai, *Compos. Sci. Technol*., **62**, 831 (2002).
19. ASTM D5045-93, *Standard Test Methods for Plane-Strain Fracture Toughness and Energy Release Rate Determination of Plastics Materials*, American Society for Testing and Materials, Philadelphia (1993).
20. B. Pukánszky and F.H. Maurer, *Polymer*, **36**, 1617 (1995).
21. A. Bezerédi, Z. Demjén, and B. Pukánszky, *Die Angewandte Makrom. Chemie*, **256**, 61 (1998).
22. M. Sakai and H. Ichikawa, *Int. J. Fract.*, **55**, 65 (1992).
23. V. Alvarez, A. Terenzi, J.M. Kenny, and A. Vázquez, *Polym. Eng. Sci.*, **44**, 1907 (2004).
24. M. Hughes, C.A.S. Hill, and J.R.B. Hague, *J. Mater. Sci.*, **37**, 4669 (2002).
25. R. Gensler, C.J.G. Plummer, C. Grein, and H.H. Kausch, *Polymer*, **41**, 3809 (2000).
26. V. Alvarez, R. Ruseckaite, and A. Vázquez, *J. Comp. Mater.*, **37**, 1575 (2003).
27. P. Montemartini, T. Cuadrado, and P. Frontini, *J. Mater. Sci.*, **10**, 309 (1999).
28. S.C. Tjong, S.A. Xu, and Y.-W. Mai, *Mater. Sci. Eng*., **A347**, 338 (2003).
29. S.G. Wong, G.X. Sui, Y. Yue, and Y.-W. Mai, *J. Mater. Sci*., **37**, 2659 (2002).
30. A. Stamboulis, C. Baillie, and E. Schulz, *Die Angewandte Makrom. Chemie*, **272**, 117 (1999).